Noninvasive Control of the Power Transferred to an Implanted Device by an Ultrasonic Transcutaneous Energy Transfer Link

Doron Shmilovitz*, *Senior Member, IEEE*, Shaul Ozeri *Member, IEEE*, Chua-Chin Wang, *senior Member, IEEE*, and Boaz Spivak

***Abstract*—Ultrasonic Transcutaneous Energy Transfer is an effective method for powering implanted devices noninvasively. Nevertheless, the amount of power harvested by the implanted receiver is sensitive to the distance and orientation of the external transmitting transducer attached to the skin with respect to the implanted receiving transducer. This paper describes an ultrasonic power transfer link whose harvested power is controlled by an inductive link. A small (5 µF) storage capacitor voltage, which is part of the implanted unit, is allowed to swing between 3.8 V and 3.5 V using hysteretic control. The two control states are indicated by excitation (while the implanted storage capacitor voltage decreases) or the absence of excitation of an implanted coil that is magnetically coupled to an external coil attached to the skin surface. A 35 mW Ultrasonic Transcutaneous Energy Transfer link was fabricated using two piezoelectric transducers of equal size (Fuji Ceramics C-2 PZT disc 15 mm × 3 mm) operated at a vibration frequency of 720 kHz. By applying the proposed hysteretic control, the captured power was effectively regulated for implantation depths of up to 85 mm.**

***Index Terms*— Ultrasonic transcutaneous energy transfer, voltage regulation, implanted medical device, hysteresis control, contactless power transfer, voltage regulation**

I. INTRODUCTION

Ultrasonic Transcutaneous Energy Transfer (UTET) is a new method to power implanted devices based on the transmission of ultrasonic energy rather than electromagnetic energy [1–4]. UTET employs an external transmitting transducer attached to the skin surface facing an implanted receiving transducer. An electrical power source energizes the transmitter, which converts the electrical energy into travelling pressure waves. The travelling pressure waves carry the energy through the tissue toward the implanted receiver positioned within the transmitter radiation lobe. The acoustic energy that reaches the receiver is converted back into electrical energy by the implanted piezoelectric transducer. An ultrasonic power transfer link can effectively transfer energy to devices implanted at distances up to 85 mm (or greater) through biological tissue. In some applications contactless energy transfer by means of ultrasound proved to be feasible even through low density medium such as air [1, 5]. Some implanted devices are miniaturized, e.g., for treating gastrointestinal and urological neuromuscular disorders [6]. To power such devices, the implanted UTET receiver should have miniaturized dimensions as well. Consequently, in these cases, the UTET receivers capture very low amounts of average power, sometimes as low as 20 µW [7]. The power harvested by the implanted receiver is used to charge a storage capacitor during the charging period until a *dc* threshold voltage level is reached. Upon reaching that level, the capacitor discharges due to the implanted device power consumption. However, the amount of energy captured by the receiver is not predictable because it is affected by factors such as the geometrical spread of the pressure wave, the accumulated power loss in the tissue, the lateral shift of the transducers with respect to one another, and the relative physical orientation of the implanted receiver with respect to the external on-skin transmitter [8].

Traditionally, inductive Transcutaneous Energy Transfer (TET) has been used to power implanted devices. A common way to control the power harvested by the receiver of an inductive link is a feedback circuit with a backward data link. For example, Baker and Sarpeshkar [9] analyzed and designed an RF power link using standard feedback control theory. They obtained a controllable, regulated output power over distances of 1–10 mm, and the output rectified *dc* voltage varied by less than 16% for distances of 2–10 mm. However, to date, no work has yet been reported on the control of a UTET link. Typically, in contactless energy transfer, with either an inductive or ultrasonic link, an *ac* voltage develops across the receiver transducer terminal with a frequency in the range of hundreds of kilohertz up to a few megahertz. Since the electronic circuitry needs a *dc* supply, the *ac* signal is rectified and filtered, and the electrical energy is stored in a capacitor (with typical values between 1 µF to 100 µF). Thus, the stored energy is controlled by controlling the voltage of

Manuscript received July 21st , 2013.

This work was supported in part by the Israel Ministry of Science under Grant number 3-7962, within the framework of the Israel and Taiwan Scientific Cooperation Program.

Doron Shmilovitz, Shaul Ozeri, and Boaz Spivak, are with the school of Electrical Engineering, Tel-Aviv University, Tel-Aviv, Israel (e-mail: shmilo@post.tau.ac.il, ozeri@post.tau.ac.il, boazsp@post.tau.ac.il).

Chua-Chin Wang is with National Sun Yat-Sen University, Kaohsiung, Taiwan (e-mail: ccwang@ee.nsysu.edu.tw).

the storage capacitor. In inductive TET, this control is typically implemented by sampling the voltage of the storage capacitor (within the implanted unit) and continuously transmitting its value to the external unit using a suitable modulation, such as amplitude shift keying (ASK) [10, 11] or frequency shift keying (FSK) [12]. While this method is adequate for relatively high power applications (i.e., above 100 mW), it occupies space within the implanted unit and consumes significant power to energize the sampling and transmission circuitry. The UTET approach was shown to be most advantageous for the transfer of relatively low power (up to tens of milliwatts) over large distances (i.e., greater than 50 mm) [1, 2]. In many cases, the power required by the implant is as low as a few milliwatts and, in some cases, even a few tens of microwatts, such as in chronic fluorescence-based biosensors [13]. Thus, since UTET-powered implants typically consume low power and are quite small, the conventional method described above has significant shortcomings for this application.

Hence, the focus of this work is a noninvasive, low-power-consumption method to sense the voltage of the implanted storage capacitor powered by a UTET. The proposed method incorporates an inductive link only for the control of the implanted storage capacitor voltage; the power transfer is performed by the ultrasonic link. The sensitivity of a UTET power transfer to various physical parameters is described first, and then, an inductive link for noninvasive control of the power is optimized to attain minimal current and real power consumption (approximately 6 mA and less than 50 µW) of the implanted control circuitry. Measurement results that fully support the proposed control method are presented.

II. INDUCTIVE LINK CONTROL OF A UTET DEVICE

UTET, in which the energy is carried by acoustic waves, is a relatively new method for transcutaneous energy transfer. In UTET, ultrasonic pressure waves are generated by an external transducer attached to the skin surface and transmitted toward an implanted transducer through the biological tissue. Only part of the transmitted energy can be captured by the implanted transducer due to loss mechanisms, such as the geometrical spread of the pressure wave, absorption and scattering in the biological tissue [18], and reflections from differing tissues and at the contact surface between the implanted transducer and the tissue. Moreover, the orientation and relative overlap of the transducers affect the energy capture as well; see Fig. 1. Fig. 2 gives the measurement results, which illustrate the influence of the distance ***z*** and the lateral shift (LS) between the transducers on the captured energy. The efficiency is defined as the ratio of the electrical power that the implanted transducer outputs, to the electrical power consumed by the transmitting transducer. The results clearly show the high dependency of the power captured on the distance and orientation of the transmitting transducer with respect to the receiving transducer. Since the power captured is sensitive to uncontrollable and potentially varying

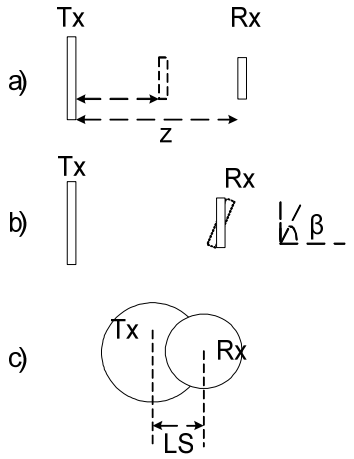

Fig. 1. Position factors that influence the power captured by the receiver. a: Distance. b: Orientation. c: Lateral shift.

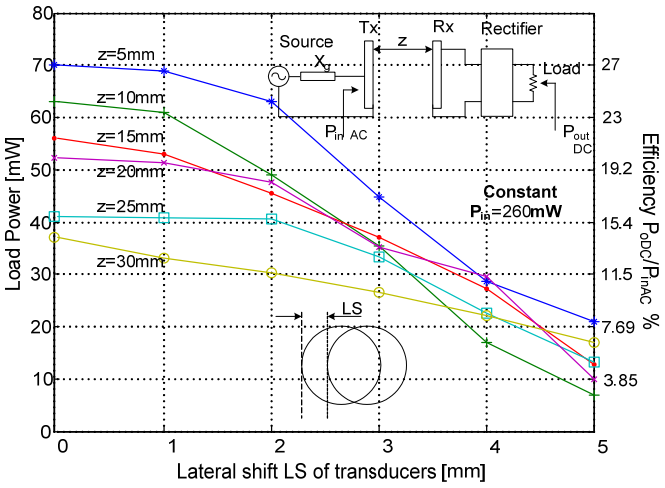

Fig. 2. Measured *dc* load power as a function of lateral shift and distance *z* (power transferred through pig muscle tissue powered by a UTET [3].

parameters such as distance, orientation, and the lateral shift between the transducers, there is an uncertainty as to the electrical energy stored in the implanted unit. Moreover, the power consumption of the implant is not constant and may vary with the operation mode. Thus, it is necessary to control the amount of energy stored in the implant.

In the proposed control method, while the power is transmitted ultrasonically, the feedback is linked magnetically. A coil is integrated with the implanted unit. When this coil is excited (by an *ac* current), a signal develops across a magnetically coupled external coil. The existence of a signal across the external coil is interpreted as a logic “1” level by the controller (within the external unit). Similarly, a “0” logic level is attained when the implanted coil is not excited and no voltage is detected across the external coil. As will be shown, this signaling method requires very low power on the implant side and is well suited to hysteretic control. A schematic illustration of a UTET controlled by the proposed hysteretic inductive link is depicted in Fig. 3. Even though the inductive link is sensitive to distance [9], lateral shift and orientation

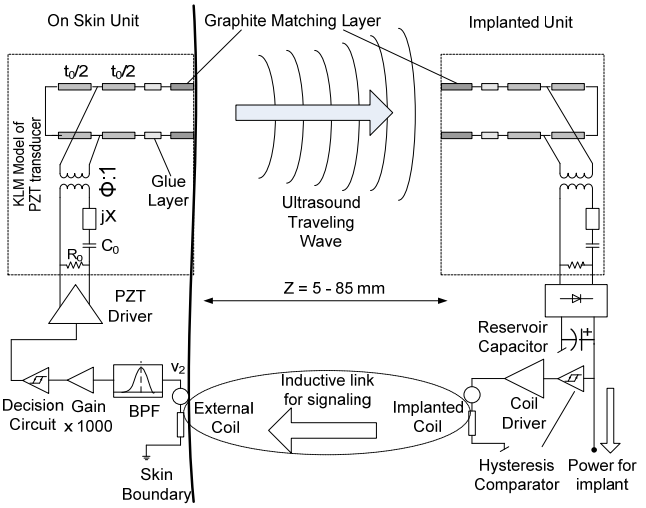

Fig. 3. Schematic of a UTET power transfer link controlled via an inductive hysteretic link.

(due to the abrupt decrease in the coupling) [14], it will be shown that, due to the binary-based signaling, it is most suitable for the transfer of the feedback signal (as opposed to the main power signal). This result is proven analytically and validated experimentally. In the following paragraph, we develop the basic computations, which indicate that a sufficiently large signal is detected by the external coil, even if the implanted coil is excited by very low currents and even for large distances between the implant and the external coil. Considering a low power implant (and, consequently, a low harvested power of, e.g., a few tens of milliwatts), the voltage sampling and feedback transmission (within the implant) must consume very low power to avoid loading the storage capacitor of the implant and reducing the energy available to energize the implant. Thus, complex modulation of the feedback is avoided, and hysteresis control is chosen. Two thresholds, V_L and V_H, are defined for the storage capacitor voltage to maintain the storage capacitor voltage between these thresholds. We set V_L = 3.5 V and V_H = 3.8 V. When the voltage of the capacitor reaches the upper bound, the internal coil is excited (by a single tone). The signal is picked by the external coil and interpreted as a logic level "1" in the external circuit. This signal commands the external unit to stop the acoustical power transmission. Thus, the storage capacitor is no longer being charged, and its voltage decays in a rhythm that depends on the power consumption of the implant. When the voltage of the storage capacitor reaches the lower bound, the implanted controller ends the excitation of the internal coil, which is interpreted by the controller (in the external unit) as a logic level of "0", thus restarting the ultrasonic energy transfer, and the charging of the storage capacitor is resumed. The main signals involved in the proposed hysteretic control are seen in Fig. 4. In addition to its simplicity, the hysteretic control adopted herein exhibits the following advantages with respect to conventional digital control:

1) During the charge periods, no signal is transmitted, and the feedback circuitry consumes negligible power.

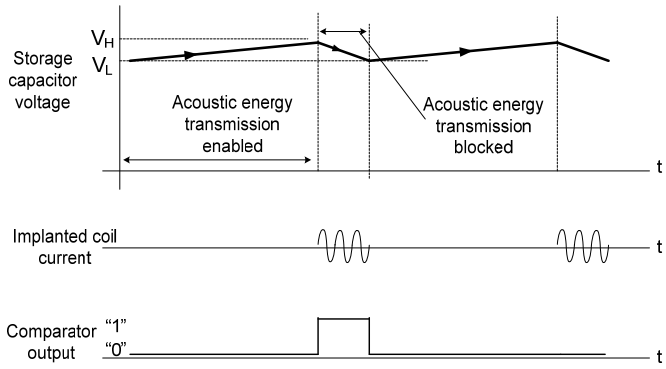

Fig. 4. Implanted storage capacitor voltage and control signals.

2) Because of the binary nature of the excitation, the feedback accuracy is unaffected by the coil relative orientation, distance, and overlapping of the coils (as long as a sufficiently high signal can be picked by the external coil terminals).
3) The approach exhibits a very fast response time (< 10 µs) because the electromagnetic signal inserts negligible delay at these distances (< 100 mm). Thus, the voltage will be well regulated, and the feedback will respond sufficiently rapidly to any perturbations.

Although the mathematical description of quasi-static inductive links is well established [9, 15], we summarize it in the following section to optimize the implanted coil design and minimize its excitation current.

A. Inductive link design

The inductive link consists of two coils; the external one is attached to the skin surface, and the second one is implanted just beneath the skin (or sometimes deeper within the soft tissue). The coils are magnetically coupled with a typically very low coupling coefficient (k < 0.1). One way to represent the inductive link is shown in Fig. 5. In this model, a voltage source feeds the primary terminals, and the primary coil is represented by its electrical impedance Z_1 and a dependent voltage source $v = j\omega M i_2$. Sometimes, a series capacitor C_s is inserted to block a *dc* voltage component that might be present at the source output. Moreover, this capacitor can be chosen to resonate with the primary inductance at the operating frequency, which allows for a reduction of the excitation voltage amplitude. The dependent voltage source in the primary network depends on the secondary current i_2, the mutual inductance M, and the angular frequency ω.

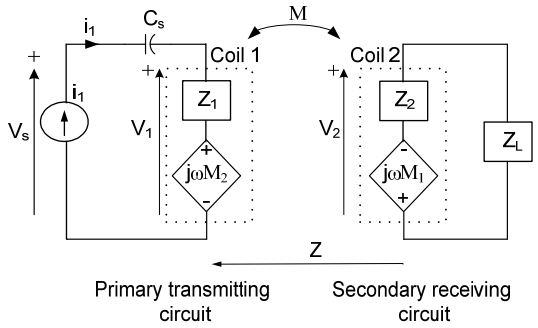

Fig. 5. A two-port model of an inductive powering link.

Similarly, the secondary circuit consists of the impedance z_2, of the secondary coil in series with a dependent voltage source that depends on the primary current i_1, on the mutual inductance M, and on the angular frequency ω.

The mutual inductance M determines the magnetic flux linkage Φ_{21} (in Weber) between the primary and secondary coils:

$$M = \frac{\phi_{21}}{i_1} \tag{1}$$

The mutual inductance M (in Henrys) depends on physical parameters, e.g., the distance between the coils, the mutual alignment of one coil with respect to the other, the diameter of the coils and the number of turns N_1 and N_2, [8] and is given in (2).

$$M = \frac{2\mu a_2 N_1 N_2}{k_0\sqrt{\rho}}\left((1-\frac{k_0^{\,2}}{2})K(k_0^{\,2}) - E(k_0^{\,2})\right) \tag{2}$$

where

$$\rho = \frac{a_2}{a_1} \tag{3}$$

$$\varsigma = \frac{z}{a_1} \tag{4}$$

$$k_0^{\,2} = \frac{4\rho}{(\rho+1)^2+\zeta^2} \tag{5}$$

where a_1 is the primary (implanted) coil diameter, a_2 is the secondary (external) coil diameter, and μ is the permeability of the soft tissue medium between the coils. It should be noted that (2) is valid under two assumptions: 1) the axial length of the coil is much smaller than its diameter, and 2) although we consider thin coils, which feature high parasitic capacitance, the capacitance may be neglected at the relatively low operation frequency of 100 kHz. The mutual inductance M, described by (2), is plotted against the distance $\boldsymbol{z}$ between the two coils and is shown in Fig. 6 for various diameters of the implanted coil a_1.

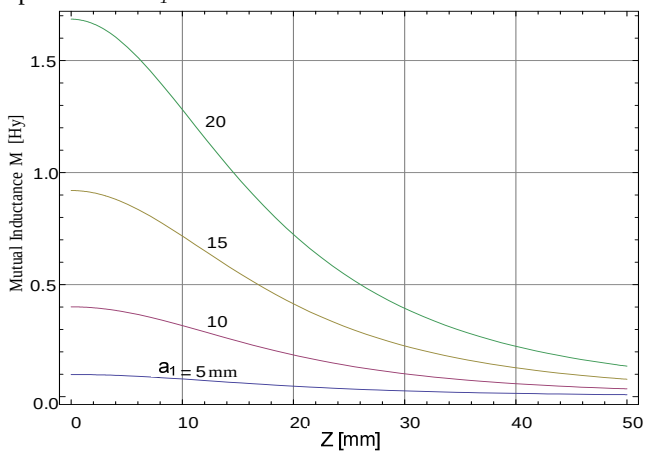

Fig. 6. Mutual inductance M as a function of the distance z between coils for various implanted coil diameters a_1. The external on-skin coil diameter a_2 is 50 mm.

Evidently, M increases with the implanted coil diameter a_1. In addition, the mutual inductance M decays rapidly as the distance $\boldsymbol{z}$ between the coils assumes a value that is close to the largest coil diameter (in this case, a 50 mm diameter external coil is used). As the distance z exceeds approximately 50 mm, the mutual inductance decreases to less than 0.25. While this value is quite low for power transfer purpose, in our case, the magnetic link serves merely for signaling. For this purpose, even a mutual inductance as low as M = 0.1 is shown to be sufficient. The relatively low signal picked up by the external coil is taken into account simply by means of a high-voltage gain amplifier (in the experiment, we used a gain of > 5000). The voltage amplitude of the received signal, v_2, increases with the excitation current and operating frequency, as depicted in Fig. 7. Fig. 7 shows that for the maximal distance of 85 mm, to attain a signal of approximately 1 mV across the secondary coil, the primary should be excited by approximately 10 mA. The received signal is applied to a voltage amplifier with a gain of approximately 5000 and then band-pass filtered (all within the external control circuitry). To achieve a sharp roll-off of the filter, a five-pole elliptic band-pass filter is used because the roll-off (transition from pass band to stop band and vice versa) sharpness of the transition band of elliptic filters is higher than that of Butterworth or Chebyshev networks. The gain ripple in the elliptic filter pass band is tolerable because the feedback signal is monotonic at 100 kHz and the feedback signaling information depends merely on the existence (= 1) or absence (= 0) of the feedback tone. The filter network and its gain response are depicted in Fig. 8. This figure shows that, the noise generated by the PZT excitation current at a frequency of 720 kHz is attenuated by more than100 dB by the elliptic band-pass filter. The filtered signal is amplified, and a decision circuit that converts the analog feedback signal into a binary signal is applied, see Fig. 9. As noted, the detected signaling level at the secondary (external) coil v_2 has an amplitude of approximately 1 mV, and the input impedance of the elliptic filter is approximately 500 ohm. Thus, the power transferred to the secondary coil is negligible (approximately 2 nW), and the implanted coil excitation power loss depends merely on the implanted coil resistance (approximately 2 Ω for the 20 turns of 32 AWG conductors,

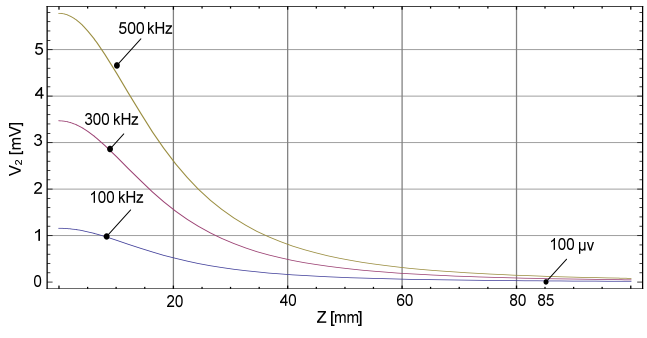

Fig. 7. Voltage developed across the external coil v_2 as a function of the distance z between coils. The implanted coil excitation was 1 mA (a_1 = 15 mm, N_1 = 20 T, N_2 = 20 T, a_2 = 50 mm). The coils are parallel and positioned coaxially.

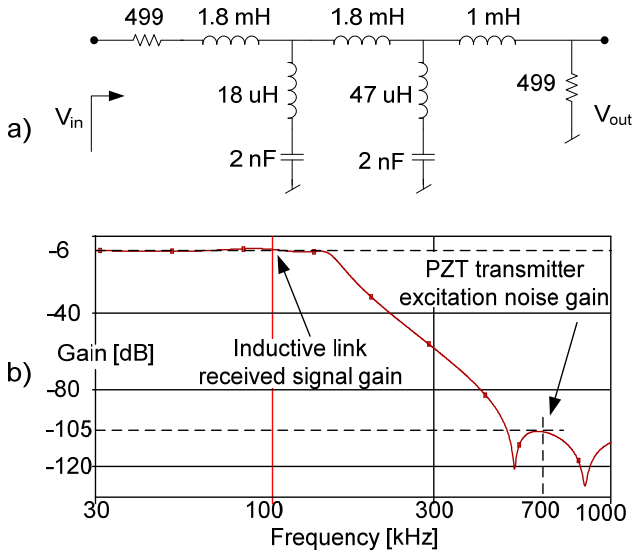

Fig. 8. Five-pole passive elliptic low-pass filter with a center frequency of 100 kHz. (a) Filter network. (b) Gain (dB).

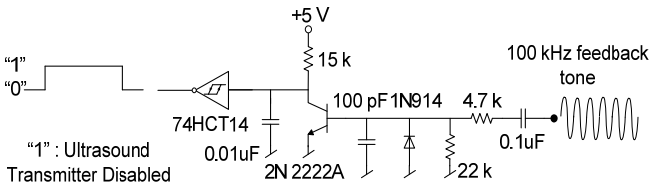

Fig. 9. Decision circuit converting feedback signals into logic levels.

including the skin and proximity effects, at 100 kHz). Thus, the excitation power loss (which is drawn from the implanted storage capacitor) is $d \bullet 50\ \mu W$ (where d is the signaling duty ratio; $0 < d < 1$). Thus, P_{loss} < 50 µW. This power is consumed only during the signaling interval of the hysteretic control, but the average power consumed for signaling is lower than 50 µW. This power can be further reduced by lowering the excitation current in the implant unit and using a higher voltage gain (> 5000) in the external controller. The following section presents considerations regarding the selection of the inductive link's signaling frequency.

B. *Inductive Link Frequency Selection*

To minimize the feedback power consumption on the implant side, an excitation current of approximately 6 mA is used. As a result, the amplitude of the received voltage v_2 is lower than 1 mV, as shown in Fig. 7. In contrast to the low signaling voltage seen at the external coil terminals, the external PZT transducer is excited by a 12 Vpk sinusoidal voltage at a frequency of approximately 720 kHz. This frequency corresponds to a resonance mode of the transducer, which is determined by its frequency constant N_t and the thickness of the PZT disc (the explicit equations governing the ratio of the ultrasonic pressure to the excitation level can be found in [16]). The PZT is connected to the external control circuit using twisted pair conductors to minimize the electromagnetic coupling to the feedback circuitry. Nevertheless, a band-pass filter is required to reject the noise at 720 kHz that may mask the low 1 mV feedback signal. To allow the use of a low-order filter, the inductive feedback operating frequency should be sufficiently far from the ultrasound frequency. The higher the frequency, the higher the received signal, v_2 amplitude; see Fig. 7. However, choosing a lower operating frequency reduces the power consumed by the implanted coil driver (which is not negligible - approximately 50 µW in this experiment). Moreover, the skin effect increases the effective resistance of the coil, therefore increasing the ohmic loss. Considering the tradeoffs involved, we applied a frequency of 100 kHz for the inductive feedback and a frequency of approximately 720 kHz for the PZT excitation.

C. *Tissue Safety Considerations*

The UTET transfers acoustic energy through the human tissue. The interaction of acoustic waves with human tissue has the potential risk of damaging the tissue through two main effects: cavitation, and thermal effect [20]. Therefore safety regulatory limits regarding the exposure of tissue to ultrasound energy must be met. The UTET is a new device thus there is no specific regulatory criteria addressing its operation. A close application category of ultrasound devices is ultrasonic imaging devices, whose safety limits [21], are adopted. The safety standards refer to two indices: Mechanical Index (MI), and Thermal Index (TI), and set limits to those indices. In order to comply with the MI and TI, we designed the UTET so as to generate an acoustic intensity below 94 mW/cm^2 (in the tissue), and choose the operating frequency in the hundreds of kHz range [2], but an accurate assessment of the tissue safety exposed to ultrasound energy is beyond the scope of this work.

III. EXPERIMENTAL SETUP AND METHOD

The main concerns in designing the inductive feedback were minimizing the power consumption and the size of the implanted coil and its associated circuitry. The transmitting coil and the feedback circuitry are fed by the storage capacitor (whose voltage is regulated), thus reducing the energy that is available to power the implanted unit circuitry. The implanted coil must not be located in front of the PZT transducer, or it may cause acoustic backward reflections of the incident ultrasonic wave due to the high acoustic impedance mismatch of the copper (33 MRayls) [17], with respect to soft tissue (approximately 1.5 MRayls) [18]. This mismatch results in a pressure reflection coefficient (for a normally incident wave) [17], Γ, of:

$$\Gamma = \left| \frac{33 - 1.5}{33 + 1.5} \right| \sim 0.913 \quad (6)$$

In this work, we used 15 mm × 3 mm (diameter × thickness) disc PZT transducers in the power transfer link. Twenty turns of 32 AWG magnet wire were wound directly over the circumference of the implanted transducer, resulting in an average coil diameter of approximately 15.5 mm. The excitation frequency of the implanted coil was chosen to be 100 kHz. At this frequency, the penetration depth is 0.2 mm (for a 32 AWG copper wire, the *ac* resistance effect begins at

approximately 200 kHz) [19]. A 32 AWG wire has a conductor radius of approximately 0.2 mm, and thus, the skin effect may be neglected. In addition, the 100 kHz frequency is lower than the low-frequency band of 120–150 kHz of radio frequency identification tags.

Measurements of the controlled UTET were performed at distances of 20, 50, and 85 mm. The external receiving coil is not limited to the footprint of the external transducer. According to (2), larger coil diameters imply a larger mutual inductance *M*; we chose the external coil diameter to be 50 mm. The external coil was located concentrically with the external PZT device, and thus, its geometric center lay on the acoustic axis common to both transducers. The dimensions and materials of the ultrasonic and inductive links used for the experiments are listed in Table I.

TABLE I
DIMENSIONS AND MATERIALS OF THE ULTRASONIC AND INDUCTIVE LINKS USED FOR THE EXPERIMENTS

	Diameter in [mm]	Number of turns and inductance	Transducer thickness in [mm]	Acoustic matching layer	Transducer material
External Transducer	15		3	Graphite	Fuji Ceramics C-2
Implanted Transducer	15		3	Graphite	Fuji Ceramics C-2
External Coil	50	20 turns L=43.4μH			
Implanted Coil	15.5	20 turns L=13.5μH			

The transducers were fabricated using 3 mm thick disc-shaped PZT elements with a diameter of 15 mm (Fuji ceramics Z3T15D). The basic transducers' parameters according to manufacturer's data are: C-2: Mechanical Quality factor Qm=1200, Coupling factor K_t=0.52, Frequency constant Nt=2020 [mHz], and Density *P*=7600[Kg/m^3]. The acoustical matching layer was fabricated from an EK2200 graphite rod (made by SGL) with a density of 1.74 [g/cm^3] and Young's modulus of 23 GPa. The graphite rod was machined to a thickness of approximately 1.4 mm The PZT disc was cleaned and wiped with acetone to remove dust and oily substance, and the graphite matching layers were bonded to it using a dual component epoxy resin Structalit 303 LV (made by Panacol, Switzerland). The actual thickness of the matching layer was calibrated experimentally to compensate for the uncertainty of the bonding layer thickness in the overall transducer impedance. To precisely characterize the transducers after fabrication, the frequency response was measured using an AP-200 frequency response analyzer (manufactured by Ridley Engineering). Fig. 10 shows the frequency response of a typical transducer. The transducer has several vibration modes: thickness vibration, radial vibration, and complex vibration modes. Each of the modes is associated with a different resonance frequency and its higher order harmonics. We operated the device at the vibration resonance of approximately 720 kHz, which is indicated by the impedance local minimum and a steep increase of the phase to

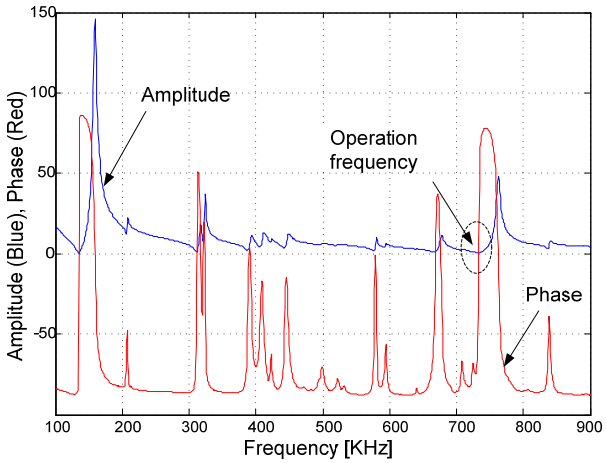

Fig. 10. Measured frequency response of an unloaded C-2 PZT element. Blue trace: absolute value of the impedance. Red trace: phase.

90°. The fabricated transducer enclosed in a Perspex housing is shown in Fig. 11. The experiments were conducted with distilled water as a medium, which closely mimics soft tissue in terms of ultrasound propagation speed and acoustic impedance. Tests were conducted inside a water-filled test tank at 25°C. The test tank dimensions were 40 cm × 20 cm × 20 cm. The tank was fabricated using 6 mm thick Perspex plates. To avoid reflections from the test tank walls, they were covered by 10 mm thick ultrasonic absorber sheets, Aptflex F28, which were attached to the internal tank walls by Aptbond B1 bond (both were manufactured by Precision Acoustics, Dorchester, UK).A manual XY manipulator (Newport Corporation M-443 series) was used to manipulate the receiver transducer location with respect to the external transducer.

Fig. 12 shows the test tank. Because the purpose of the experiment was to present a noninvasive control method of the implanted storage capacitor voltage, the UTET link was not optimized for power transfer efficiency. To simplify the experimental setup, we used distilled water, although degassed water would have been more appropriate because dissolved gas in the medium may block and scatter part of the ultrasonic wave energy due to the cavitation effect, especially near the radiating transducer surface, where the wave intensity attains its maximum value. The control circuitry consists of implanted low-power electronic circuitry and external circuitry.

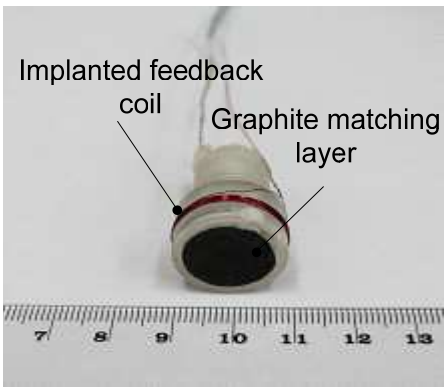

Fig. 11. Photograph of the fabricated PZT transducer.

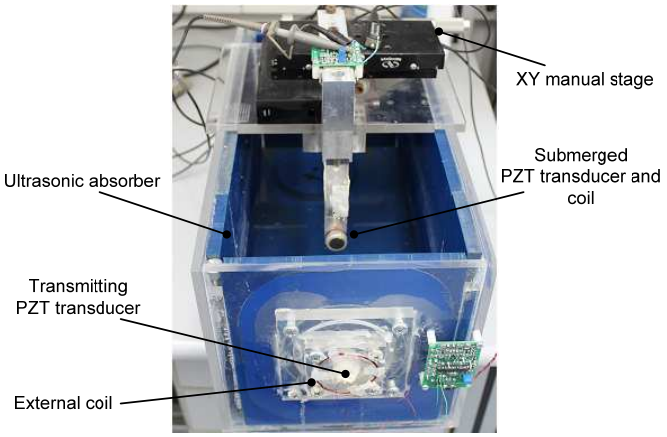

Fig. 12. Photograph of the ultrasonic test tank.

The hysteretic control was implemented using a low-power analog comparator (TI LMV7271, with a 5 µA current consumption and approximately 1 µs propagation delay) and a 1.2 V +/− 0.5% µ-power voltage-reference (Analog Devices AD1580). A conceptual scheme of the implanted control circuit is depicted in Fig. 13. In the experiment, an implanted storage capacitor of 5 µF (X7R dielectric) was charged (by the power captured by the implanted PZT transducer). The capacitor voltage was compared with two threshold voltages, 3.8 V and 3.5 V. During the charge phase, the capacitor voltage ramps up. When it hits the upper bound, the comparator output flips and triggers the implanted coil's excitation. This transmission commands the external transmitter to cease the ultrasound power transmission. At this time, the capacitor is not being charged; however, it still supplies the implanted circuit with power (responsible for its functionality) and the power consumed by the hysteretic control and the excitation of the coils. Thus, the voltage on the capacitor starts to ramp down. When the capacitor voltage reaches the lower bound, the output of the comparator flips, the ultrasonic transmission resumes, and the capacitor starts charging. The storage capacitance, the amount of power captured by the receiver, and the implanted load consumption determine the charge rhythm of the capacitor and its voltage ripple frequency.

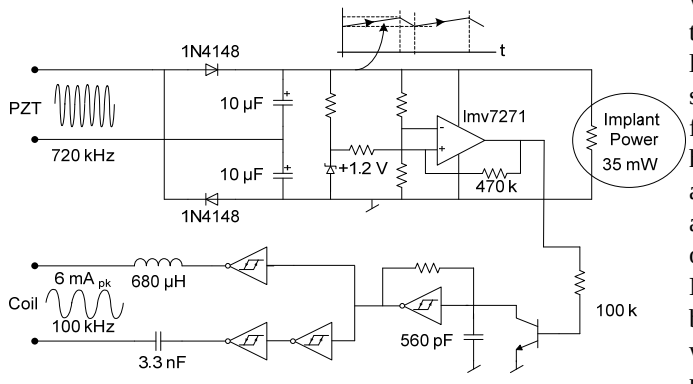

Fig. 13. General description of the feedback circuitry.

The discharged energy during the maximal voltage drop is:

$$E = P_{load} \cdot t_{off} = 0.5 \cdot C\left(V_H{}^2 - V_L{}^2\right) \ . \qquad (7)$$

For an implanted load consuming 35 mW, the voltage fall time is given by (8).

$$t_{off} = 0.5 \cdot C\left(V_H{}^2 - V_L{}^2\right) / P_{load} = \\ = 0.5 \cdot 5\mu\left(3.8^2 - 3.5^2\right) / 0.035 = 156\mu s \qquad (8)$$

Initially, the implanted transducer was located inside the water tank on the acoustic axis of the external transducer.

The maximum distance of 100 mm was determined by finding the point at which the power captured was barely sufficient to charge the storage capacitor to the upper threshold V_H = 3.8 V, while the external transducer was constantly excited (12 Vpk), i.e., an energy duty cycle equal to 1. The maximum distance was practically limited to z = 85 mm because the inductive link was insufficiently powerful beyond 85 mm (this range could be extended by increasing the implanted coil excitation current or by increasing the voltage gain in the external receiver). Starting from z_{max} = 85 mm, the distance was reduced gradually, using the XY manipulator, until a minimal distance of z_{min} = 20 mm. The inductive control maintained the storage capacitor voltage within the range z_{max} to z_{min}.

IV. EXPERIMENTAL RESULTS AND DISCUSSION

A UTET system controlled by an inductive link based on hysteresis control, as illustrated in Fig. 3, was constructed and operated within a test tank, as described previously. The external control circuitry was connected to a *dc* voltage source, which was the sole power source that fed the system (both the external and internal parts). The implanted control circuitry was fed by the energy storage capacitor, whose energy came from the power harvested by the implanted ultrasonic transducer. The voltage of the 5 µF implanted storage capacitor, regulated through the inductive link, is shown in Fig. 14 for an implanted load with a power consumption of 35 mW and implant depths of 50 mm and 85 mm. The power captured by the implanted transducer at a distance of 85 mm is less than the power captured at 50 mm, mainly because of the geometric spread of the ultrasonic wave. The power loss is less affected by attenuation because the medium used in the experiment was water, which has a lower ultrasound attenuation at 720 kHz (< 0.01 dB/cm) than soft tissue (approximately 1–3 dB/cm) [18]. The voltage ripple frequency on the storage capacitor depends on the power harvested. According to Fig. 14, the ripple frequency was approximately 330 Hz at 85 mm and approximately 1500 Hz at 50 mm. A lower harvested power causes a longer duration of the voltage ramp up until the upper threshold is reached. Meanwhile, the voltage fall time remains nearly constant because it depends on the load power consumption, which was not changed throughout the experiment (a total of 35 mW, out of which approximately 50 µW went to the implanted coil excitation).

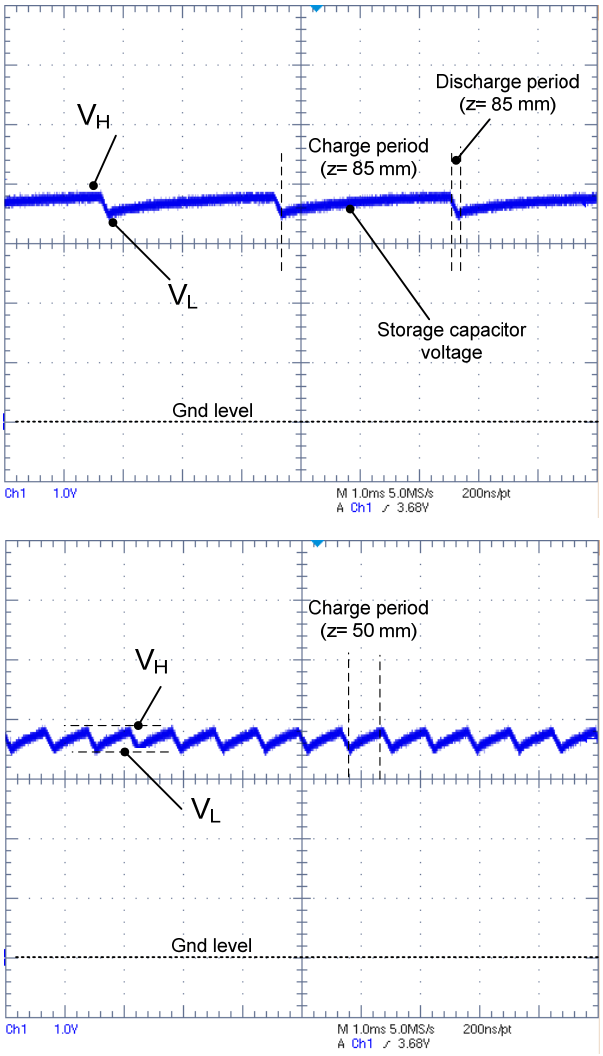

Fig. 14. Implanted storage capacitor voltage at a distance of 85 mm (upper) and 50 mm (lower). The harvested power is 35 mW.

The storage capacitor voltage is regulated by a low dropout regulator that provides a stable output voltage of 3.3 Vdc. The frequency of the ripple superimposed on the *dc* level is sufficiently low to be effectively attenuated by the low dropout because of its high power supply rejection ratio (> 60 dB). The storage capacitor voltage and the excitation of the implanted coil are shown in Fig. 15. As seen in Fig. 15, the implanted coil is excited only during the voltage decay, thus saving energy during the periods in which the energy stored in the capacitor is low. The excitation current amplitude of the coil is approximately 6 mA, and it persists as long as the voltage falls (but is still above the lower voltage threshold of V_L = 3.5 V). Thus, the excitation power required for the inductive link is drawn from the storage capacitor only while there is sufficient energy accumulated in the implanted storage capacitor.

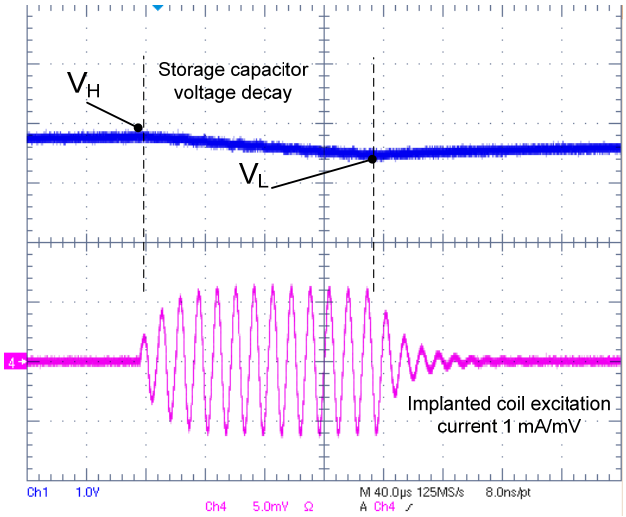

Fig. 15. Storage capacitor voltage (upper trace) and implanted coil excitation (lower trace) at a distance of 85 mm between the transducers.

For a 35 mW load power (representing the implanted circuitry power consumption and the coil excitation power, which is also drawn from the capacitor), the voltage fall time rate is approximately 2.5 mV/µs. Fig. 16 shows the storage capacitor voltage, the implanted coil excitation current, the external ultrasonic transducer excitation voltage, and the propagating ultrasonic wave flowing in the medium. The propagating ultrasonic wave was measured by a hydrophone (TC4038, manufactured by Reson, Denmark, with a sensitivity of −228 dB +/− 2 dB re 1 V/µPa at 100 kHz). The excitation of the ultrasonic transducer was implemented by a self-fabricated switched-mode driver, in which the switches were implemented by a MOSFET driver (MIC 4126). The driver generated a voltage pulse train at a frequency equal to the resonance frequency of the PZT transducer. The square wave pulse train was shaped by an LC network (6.8 µH, 3.9 nF) to achieve a sinusoidal voltage for the excitation of the PZT transducer (the PZT transducer should be excited by a highly sinusoidal voltage to avoid excitation of its higher-order vibration modes). Fig. 17 depicts the power driver and the excitation voltage waveforms. The voltage regulation accuracy is degraded because of the accumulated time delays inserted by the ultrasonic and inductive links. The time delay due to ultrasonic wave propagation through a distance of approximately 35 mm may be deduced from Fig. 18. The lower signal (magenta) is the MOSFET driver–generated pulse train, while the storage capacitor voltage drops. The sinusoidal excitation voltage (blue) on the terminals of the transducer follows the pulse train after a small delay resulting from the LC filter (that filters out the pulse train harmonics). Because of the low speed of sound in water (approximately 1500 m/s at 25°C, [18], the ultrasonic wave reaches the implanted transducer 24 µs after the external piezo driver starts to energize the external PZT transducer.

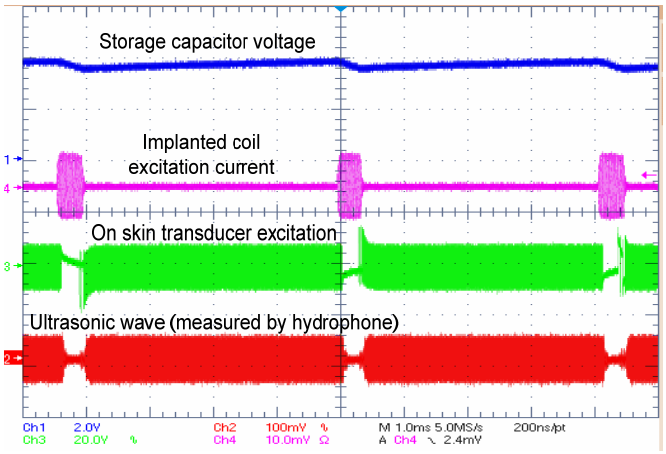

Fig. 16. Main signals of the system: storage capacitor voltage (upper blue trace), excitation current of the implanted coil (magenta trace), excitation voltage of the external ultrasonic transducer (green trace), and the ultrasonic wave measured at a distance of 50 mm from the transmitter.

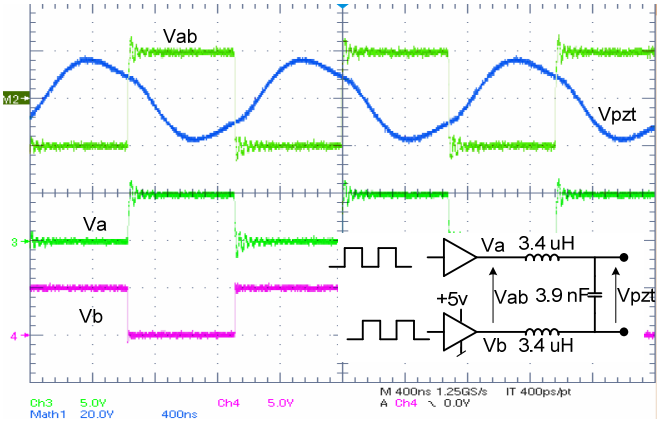

Fig. 17. PZT excitation voltage generated by the MOSFET driver.

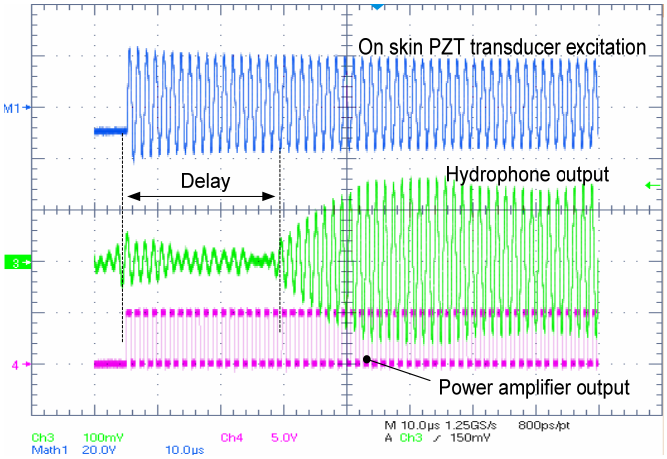

Fig. 18. Propagation delay for a distance of 35 mm (transducer excitation triggered when the storage capacitor voltage reached the lower threshold V_L): power amplifier generated pulse train (magenta), sinusoidal excitation applied to the external transducer (trace), and resulted ultrasonic wave (green).

This delay depends on the distance between the transducers and reaches approximately 56 µs for a distance of 85 mm. The storage capacitor continues to discharge until the ultrasonic wave reaches the front surface of the implanted transducer and the capacitor starts to recharge. For a load power consumption of 35 mW, the voltage decay rate is approximately 2.5 mV/µs, which means that the capacitor actually discharges to a voltage of 2.5 mV/µs · 56 µs = 0.144 V below the lower threshold voltage V_L. This error voltage can be compensated by presetting the lower voltage threshold to a slightly higher level.

Regarding the influence of the PZT transducers on the inductive link signals, the back and front surfaces of the PZT transducers are covered by a thin (10 µm thick) silver coating, which forms the electrodes. Both the PZT material and the conducting electrodes may adversely influence the magnetic link. To measure the influence of the PZT transducer on the inductive link, a measurement setup was constructed that consisted of a transmitting coil and a receiving coil at a distance of 50 mm. The size and number of turns of the coils were similar to those in the main experiment. The implanted coil was excited by a 5 mA sinusoidal current at 100 kHz. The influence of the ultrasonic transducers composed of hard PZT and graphite acoustical matching layers on the inductive link feedback amplitude was measured by comparing the signal detected at the external coil in the absence of the ultrasonic transducers with the signal developed in its presence. This process was repeated for frequencies of 100 kHz to 1 MHz. To increase the measurement sensitivity, a voltage amplifier with a 20 dB gain was used to amplify the received signal that developed on the external coil (Reson, VP 1000 voltage amplifier). The measured attenuation is depicted in Fig. 19. The results show that at 100 kHz (the chosen signaling frequency), the presence of the transducers contributes less than 1% to the voltage attenuation in the inductive link feedback. The attenuation increases to approximately 9% for a signaling frequency of 1 MHz. It is assumed that the attenuation is caused mainly by eddy currents induced in the transducer electrodes. An accurate assessment of the interaction between the silver-coated PZT and graphite matching layer materials with the alternating magnetic fields is beyond the scope of this paper. At 100 kHz, the inductive link signaling frequency that we chose, the attenuation is negligible, so it minimally contributes to the power consumption of the inductive link.

V. CONCLUSIONS

A noninvasive method of control for UTET was proposed and characterized. The main aspects considered were presented, and design guidelines were derived.

The voltage regulation method is based on hysteretic control of the implanted storage capacitor voltage by maintaining its voltage between an upper voltage bound of 3.8 V and a lower voltage bound of 3.5 V. The implant unit signals the external power transmitter to momentarily cease ultrasonic power transmission via an inductive link. An implanted coil with 20 turns wound over the circumference of the implanted PZT transducer is excited by a 6 mA 100 kHz sinusoidal current when the implanted capacitor voltage reaches its upper bound. The feedback signal transmitted by the implanted coil is detected by an external coil, which stops the ultrasonic power transmission.

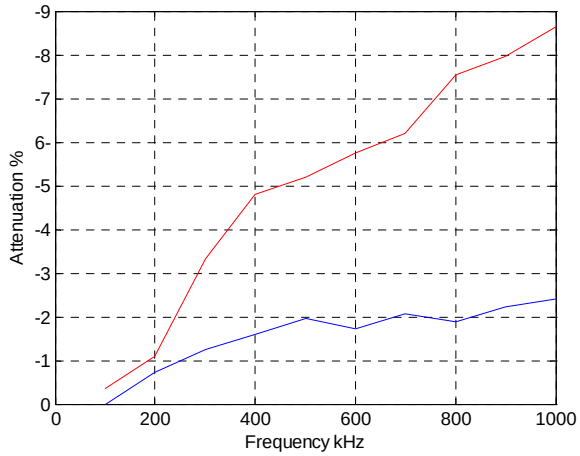

Fig. 19. Masking of the inductive link signal by the ultrasonic transducers within the alternating magnetic field of the inductive link. Red: attenuation by implanted transducer. Blue: attenuation by external on-skin transducer.

The avoidance of complicated sample and transmission circuitry is significant for saving power and space within the implanted unit. The average power consumption of the implanted signaling circuitry, including the coil excitation power, is less than 50 μW. The proposed inductive link hysteretic control method was demonstrated successfully with a UTET system operated in an ultrasonic test tank for a distance range of 20 mm to 85 mm between the implanted unit and the external unit.

REFERENCES

[1] M. G. L. Roes, J. L. Duarte, M. A. M. Hendrix and E. A. Lomonova, "Acoustic Energy Transfer: A Review," *Industrial Electronics, IEEE Transactions on*, vol. 60, pp. 242-248, 2013.

[2] S. Ozeri, D. Shmilovitz, "Ultrasonic transcutaneous energy transfer for powering implanted devices," *Ultrasonics*, vol. 50, pp. 556-566, 2010.

[3] S. Ozeri, D. Shmilovitz, S. Singer, C. C. Wang, "Ultrasonic transcutaneous energy transfer using a continuous wave 650 kHz Gaussian shaded transmitter," *Ultrasonics*, vol. 50, pp. 666-674, 2010.

[4] Y. Shigeta, T. Yamamoto, K. Fujimori, M. Sanagi, S. Nogi and T. Tsukagoshi, "Development of ultrasonic wireless power transmission system for implantable electronic devices," *Wireless Technology Conference, 2009. EuWIT 2009. European*, pp. 49-52, 2009

[5] M. G. L. Roes, M. A. M. Hendrix and J. L. Duarte, "Contactless energy transfer through air by means of ultrasound," *37th Annual Conference on IEEE Industrial Electronics Society, IECON* 2011, pp. 1238-1243.

[6] J. A. Doherty, G. A. Jullien and M. P. Mintchev, "Transcutaneous powering of implantable micro-stimulators for functional restoration of impaired gastrointestinal motility," in *Engineering in Medicine and Biology Society, 2003. Proceedings of the 25th Annual International Conference of the IEEE*, 2003, pp. 1575-1578 Vol.2.

[7] R.F. Xue, J. H. Cheong, H. K. Cha, X. Liu, P. Li, H. J. Lim, L. S. Lim, M. Y. Cheng, C. He, W. T. Park, M. Je, "Ultra low power implantable blood flow sensing microsystem for vascular graft ", 13th international symposium on integrated circuits ISIC, pp. 224-220, Dec. 2011.

[8] S. Ozeri, B. Spivak, D. Shmilovitz, "Non-invasive sensing of the electrical energy harvested by medical implants powered by an ultrasonic transcutaneous energy transfer link", *IEEE international symposium on industrial electronics ISIE*, pp. 1153-1157, 2012.

[9] M. W. Baker and R. Sarpeshkar, "Feedback Analysis and Design of RF Power Links for Low-Power Bionic Systems," *Biomedical Circuits and Systems, IEEE Transactions on*, vol. 1, pp. 28-38, 2007.

[10] C.C. Wang, C.L. Lin, R.C. Kuo, and D. Shmilovitz, "Self-sampled all-MOS ASK demodulator for lower ISM band applications," *IEEE Trans. Circuits Syst. II*, vol. 57, no. 4, pp. 265-269, Apr. 2010.

[11] C.-C. Wang, T.-J. Lee, and Y.-J. Ciou, "C-less and R-less low-frequency ASK demodulator for wireless implantable devices," in Proc. *IEEE Int Symp. Integr. Circuits*, vol. 1, pp. 604–607. Sep. 2007

[12] J. Abouei, J. D. Brown, K. N. Plataniotis and S. Pasupathy, "Energy Efficiency and Reliability in Wireless Biomedical Implant Systems," *Information Technology in Biomedicine, IEEE Transactions on*, vol. 15, pp. 456-466, 2011.

[13] P. Valdastri, E. Susilo, T. Forster, C. Strohhofer, A. Menciassi and P. Dario, "Wireless Implantable Electronic Platform for Chronic Fluorescent-Based Biosensors," *Biomedical Engineering, IEEE Transactions on*, vol. 58, pp. 1846-1854, 2011

[14] C. M. Zierhofer and E. S. Hochmair, "Coil design for improved power transfer efficiency in inductive links," in *Engineering in Medicine and Biology Society, 1996. Bridging Disciplines for Biomedicine. Proceedings of the 18th Annual International Conference of the IEEE*, 1996, pp. 1538-1539 vol.4.

[15] Uei-Ming Jow and Maysam Ghovanloo, "Modeling and optimization of printed spiral coils in air, saline, and muscle tissue environments," IEEE Trans. Biomed. Circuits Syst., vol. 3, no. 5, pp. 339–347, October 2009

[16] R. Krimholtz, D.A. Leedom, G.L. Mattaei, "New equivalent circuits for elementary piezoelectric transducer", Elect. Lett. 6, pp. 398–399, 1970.

[17] D. T. Blackstock, "Physical acoustics", John Wiley Pub., 2000, pp.39–44, pp. 130-134, pp. 511.

[18] Francis A Duck, Andrew C Baker and Hazel C Starritt, "Ultrasound In Medicine", Institute of Physics Publishing 1998, pp. 73-79.

[19] O. M. O. Gatous and J. Pissolato, "Frequency-dependent skin-effect formulation for resistance and internal inductance of a solid cylindrical conductor," *Microwaves, Antennas and Propagation, IEE Proceedings*, vol. 151, pp. 212-216, 2004.

[20] S. B. Barnett, H. D. Rott, G. R. T. Haar, M. C. Ziskin, K. Maedaii, "The sensitivity of biological tissue to ultrasound", *Ultrasound in Med & . Biol.*, vol. 23, no. 6, pp. 805-812, 1997.

[21] U.S. Department of Health and Human Services, Food and Drug Administration, Center for Devices and Radiological Health, "Information for manufacturers seeking marketing clearance of diagnostic ultrasound systems and transducers," Sept. 9 ,pp. 1-64 2008.